Received: 5 April 2019 | Revised: 21 May 2019 | Accepted: 22 May 2019

DOI: 10.1111/jace.16608

ORIGINAL ARTICLE

Journal of the American Ceramic Society

Grain boundary curvatures in polycrystalline $SrTiO_3$: Dependence on grain size, topology, and crystallography

Xiaoting Zhong | **Madeleine N. Kelly** | **Herbert M. Miller** | **Shen J. Dillon** | **Gregory S. Rohrer**

Department of Materials Science and Engineering, Carnegie Mellon University, Pittsburgh, Pennsylvania

Correspondence
Gregory S. Rohrer, Department of Materials Science and Engineering, Carnegie Mellon University, Pittsburgh, PA 15213.
Email: gr20@andrew.cmu.edu

Present Address
Herbert M. Miller, Bettis Laboratory, Naval Nuclear Laboratory, West Mifflin, Pennsylvania

Shen J. Dillon, Department of Materials Science and Engineering, University of Illinois Urbana-Champaign, Urbana, Illinois

Funding information
W. M. Keck Foundation; Carnegie Mellon University, Grant/Award Number: MCF-677785; Division of Materials Research, Grant/Award Number: 1428480 and 1628994

Abstract

By mapping grain orientations on parallel serial sections of a $SrTiO_3$ ceramic, it was possible to reconstruct three-dimensional orientation maps containing more than 3000 grains. The grain boundaries were approximated by a continuous mesh of triangles and mean curvatures were determined for each triangle. The integral mean curvatures of grain faces were determined for all grains. Small grains with fewer than 16 neighbors mostly have positive mean curvatures while larger grains with more than 16 neighbors mostly have negative mean curvatures. It is also possible to correlate the mean curvature of individual triangles with the crystallographic characteristics of the grain boundary. The mean curvature is lowest for grain boundaries with (100) orientations and highest for grain boundaries with (111) orientations. This trend is inversely correlated to the relative areas of grain boundaries and directly correlated to the relative grain boundary energy. The direct correlation between the energy and curvature is consistent with the expected behavior of grain boundaries made up of singular orientations. Furthermore, because both the relative energy and curvature of grain boundaries with (100) orientations are minima in the distributions, these boundaries also have the lowest driving force for migration.

KEYWORDS

grain boundaries, microstructure, strontium titanate

1 | INTRODUCTION

Grain growth occurs through the motion of individual grain boundaries and the rate of grain growth is determined by the grain boundary velocity (v) at a specific temperature and pressure. The general expression for the boundary velocity[1,2] at a point i is:

$$v_i = M_i \left[\left(\gamma_i + \frac{\partial^2 \gamma_i}{\partial \theta_1^2} \right) \kappa_1 + \left(\gamma_i + \frac{\partial^2 \gamma_i}{\partial \theta_2^2} \right) \kappa_2 \right] \quad (1)$$

This expression applies to each point of interest where γ_i is the grain boundary energy at that point, M_i is the grain boundary mobility, and κ_1 and κ_2 are the principal curvatures. The derivatives with respect to θ_1 and θ_2 measure the changes in surface energy with respect to changes in the orientation of the surface normal in the two principal directions. The expression in Equation 1 is difficult to use in practice because grain boundary energies and mobilities vary with grain boundary crystallography. Grain boundary energies vary with lattice misorientation and grain boundary plane orientation[3] and mobilities vary with lattice misorientation.[4–6] As a result, Equation 1 is rarely used.[7] More commonly, it is applied in the following simplified form:

$$v = \langle M \rangle \langle \gamma \rangle H \quad (2)$$

where H is the mean curvature ($H = 1/2(\kappa_1 + \kappa_2)$) and $<M>$ and $<\gamma>$ are averages over the variations that occur for grain boundaries with different crystallographic parameters (note that throughout this document, we generally refer to mean curvature simply as curvature). While this might be a reasonable approximation in some cases, it often fails to predict the motions of specific boundaries.[8,9]

Of these physical quantities, perhaps the least is known about the curvature. In most work, H is assumed to be the inverse of the mean spherical equivalent grain radius. With the emergence of three-dimensional microscopic techniques and simulations, it has become possible to locally measure curvature within voxelized microstructures[10–15] and a technique that can be used to measure local grain boundary curvature and correlate it to the crystallography of the grain boundary has recently been reported.[16] The method has been applied to two ferrous alloys and it was found that the curvature varies strongly as a function of the grain boundary plane orientation. Here, we apply the same technique to a ceramic ($SrTiO_3$) and explore in more detail the correlations among the grain boundary relative area, energy, and curvature.

$SrTiO_3$ was selected for this study for two reasons. First, we already have some knowledge of the types of grain boundaries that exist in $SrTiO_3$ and their energetics.[17–19] Second, there is considerable current interest in grain boundary motion in $SrTiO_3$ because of the grain growth anomaly that occurs in the temperature range of 1350°C to 1425°C.[20–24] In this temperature region, the grain growth rate constant decreases by two orders of magnitude, while in most cases the grain growth rate constant is expected to increase with temperature.[22] The decrease in the rate constant is the result of an increasing concentration of relatively slowly moving grain boundaries. There is also a change in the distribution of grain boundary planes, with the fraction grain boundaries with the (100) orientation increasing in the region where the grain growth rate constant decreases.[17] In the same temperature range, there is a decrease in the grain boundary energy.[25] These observations have been interpreted as evidence for a grain boundary structural transition. However, microscopic studies of the boundaries do not provide strong evidence for such a transition.[26–28] Shih et al[26] reported a tendency for larger grains to have atomically flat (100) oriented grain boundaries. Sternlicht et al noted no difference in the structure of the fast moving and slower boundaries.[28] The same group reported that the boundaries move by the motion of steps and that on the microscopic level, the boundaries were made up of a limited number of low index atomically flat orientations.[27,28]

The purpose of this paper is to describe the distribution of grain boundary characters, grain boundary energies, and grain boundary curvatures as function of the five crystallographic parameters in $SrTiO_3$. We have used three-dimensional electron backscattered diffraction (3D-EBSD) to determine the orientations and shapes of more than 3000 grains. The relative areas and curvatures of different types of boundaries have been measured. Assuming local equilibrium at triple lines, the geometries of tri-grain junctions were used to approximate the relative grain boundary energy. It has been found that grain boundary curvatures not only depend on the crystallography of the grain boundary, they are also correlated to the relative areas and the relative grain boundary energies.

2 | EXPERIMENTAL METHODS

A polycrystalline ceramic was prepared from commercially available $SrTiO_3$ powder (Sigma-Aldrich Corp., St. Louis, MO, 99% pure). The powder was dry-ground for approximately 10 minutes in an alumina mortar and uniaxially compacted at 1000 psi to form a 1⁄2" diameter pellet. The pellet was fired in air in a box furnace (Lindberg/Blue M 1700°C box furnace, Riverside, MI) according to the following heating schedule. The furnace was heated at 10°C/min to 900°C. After a 10 hours dwell, it was heated at 5°C/min to 1340°C. After another 10 hours dwell, it was heated at 20°C/min to 1470°C, held at that temperature for 30 minutes, and then furnace cooled to room temperature.

3D-EBSD data were collected using procedures that have already been described in detail.[29] The sample was milled with a Ga^+ion focused ion beam (Nova 600, FEI Co., Hillsboro, OR) and the backscattered diffraction patterns were collected using an EBSD detector (EDAX, Mahwah, NJ). The sample was ion milled at 30 kV and 3 nA and the EBSD data were acquired on a hexagonal grid using a 30 kV beam at a current of 9.5 nA.

The design of the heat treatment and the choice of EBSD parameters were determined from the requirement that the data should cover thousands of grains, which is necessary for analyzing the distribution of grain boundary properties as a function of the five independent crystallographic parameters. To obtain data from this many grains in a reasonable period of time, one must consider the spatial resolution of EBSD orientation maps, the amount of time it takes to record the orientation maps, and the amount of time it takes to remove a layer of material by serial sectioning. The latter two parameters are characteristics of the instrument; for the instrument used for this study, we were limited to samples with average grain diameters between 1 and 5 μm (although for more modern instruments, the upper bound on the grain size has increased considerably). The limits arise because if the grains are too small, it is not possible to resolve the interface shapes and if the grains are too large, the rate of ion milling and data acquisition make the length of the experiment impractical. The in plane EBSD resolution was 300 nm and the

spacing between layers was also 300 nm. Two volumes were collected, one consisting of 36 layers and another consisting of 40 layers.

In the first step, the data were cropped and cleaned using the TSL OIM software. Each area in the two volumes was cropped to 69.3 μm × 38.4 μm or 63.6 μm × 76.8 μm. The EBSD data were cleaned using two iterations of grain dilation with a minimum grain size of 10 pixels. This procedure considers any grouping with fewer than 10 pixels, or disorientations of <5°, to be insufficient to define a grain and assigns their orientation to match the orientation of an adjacent grain. A single average orientation was assigned to each grain, with an individual grain being defined as a set of pixels whose disorientations lie within 5° of one another. These maps were used as the input for the remainder of the analysis.

To measure the grain boundary character distribution (GBCD), which is the relative areas of grain boundaries as a function of the boundary misorientation and boundary plane orientation, and the grain boundary curvature distribution (GBHD), which is the unsigned mean curvature of grain boundaries as a function of the same five parameters, it is necessary to reconstruct the 3D interface structure. These steps are all carried out using open source software DREAM.3D version 6.4.[30] All of the procedures are similar to those used in Ref. [31] and are briefly outlined here. The first step of reconstruction is to stack the 2D serial sections together to create continuous 3D volumetric data. To do this, it is necessary to correct unavoidable small misalignments between the sections and points in the maps where the orientations were not reliably determined (based on the confidence index (CI) assigned by the OIM software). Vertically adjacent sections were aligned to minimize the misorientations between the sections and voxels with low CI orientations were replaced by the orientations of its more reliable nearest neighbor voxels using the rule of majority vote. The microstructure was segmented into grains by grouping contiguous voxels with similar orientations (<5°) and assigning them a unique identification number (ID). After segmentation, DREAM.3D also makes it possible to compute microstructure statistics such as grain sizes, average grain orientations, and number of neighbors, for example.

Within DREAM.3D, a grain boundary is the interface between the segmented grains. Because of the terrace-step geometry of the interface created by the cube-shaped voxels, these interfaces are poor imitations of real grain boundaries, which are presumed to be smooth on a micron length scale. To create smoother interfaces, we used the quick mesh filter, followed by the Laplacian smoothing filter. After these operations, the interfaces are represented by a collection of triangles forming a continuous mesh. The mesh covered approximately 19 000 grain faces and was made up of 2 800 000 triangular grain boundary patches. For each triangle, we know the orientation of the grain on either side of the triangle, the triangle's orientation, its area, and its mean curvature. The triangle mean curvature was calculated from a least-squares fit method using the second and third neighborhood of the central triangle. The details are described in Refs. [16,32]. It is then possible to examine the relative areas and absolute curvatures of the boundaries as a function of the five crystallographic parameters that describe the grain boundary. It is also possible to add the curvatures of the triangles bounding a single grain to determine the integral mean curvature of grain faces (M_s) for each grain. Note that extreme mean curvature values also exist because of imperfect mesh quality, especially at triple lines and quadruple points. Because these values are thought to be nonphysical, curvatures with a magnitude greater than $\pm 100\ \mu m^{-1}$ were excluded from the mean curvature calculation.

The relative grain boundary energies were estimated using the method developed by Morawiec.[33] The method is based on the assumption that the triple junctions are in local thermodynamic equilibrium and that this equilibrium is described by the Herring[34] equation. In Morawiec's method, the Herring equilibrium is expressed as a vector equation using Hoffman and Cahn's capillarity vector:[35,36]

$$\left(\vec{\zeta}^1+\vec{\zeta}^2+\vec{\zeta}^3\right)\times\vec{l}=0 \tag{3}$$

here, $\vec{\zeta}^i$ are the capillarity vectors associated with the three grain boundaries and $\vec{l}$ is the direction of the triple line. As explained in detail in Ref. [33], the component of $\vec{\zeta}$ perpendicular to the boundary is $\overrightarrow{\zeta_\perp}=\gamma\left(\vec{n}\right)\vec{n}$, where $\gamma\left(\vec{n}\right)$ is the inclination dependent energy for that boundary and $\vec{n}$ is the surface normal. The component of $\vec{\zeta}$ parallel to the boundary is $\overrightarrow{\zeta_\parallel}=(\partial\gamma/\partial\beta)_{\max}\vec{t}$. Here, $\vec{t}$ is a vector tangent to the surface and β is a right-handed angle of rotation about $\vec{l}$. The experimental observables are $\vec{l}$, $\vec{n}$, and $\vec{t}$; the unknowns are the scalar components of $\vec{\zeta}$. The five-dimensional space of grain boundary characters was discretized with 9 bins per 90° using procedures described in detail elsewhere[19,37] and each discrete bin is associated with a capillarity vector. An iterative procedure is then used to find the set of capillarity vectors that most nearly satisfies this system of linear equations (33). In the present case, we have 21,698 observed triple junctions and the distribution converged after 200 iterations using a relaxation factor of 0.1 (here, the condition for convergence is that the change on the last iteration is less than 1% of the change in the first iteration). The energies are relative to one another and normalized so that the average is unity. We therefore named the units of the energy "relative units (r.u.)."

3 | RESULTS

Two volumes of the $SrTiO_3$ ceramic and an example of a reconstructed grain, showing the triangular mesh representing

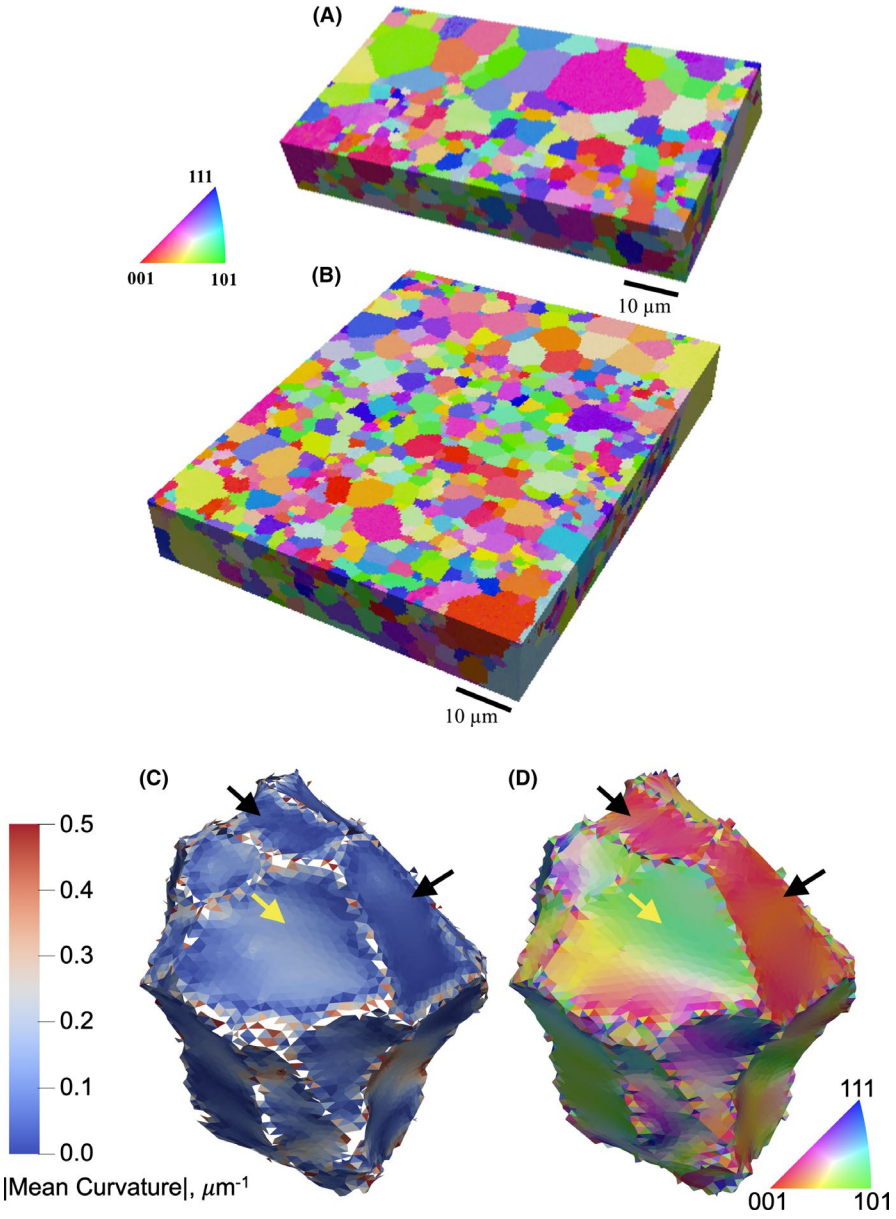

FIGURE 1 Two volumes of $SrTiO_3$ and a reconstructed grain. (A) 69.6 μm × 38.7 μm × 10.8 μm (B) 63.9 μm × 89.1 μm × 12 μm. The grains in (A) and (B) are colored by orientation, according to the color key. (C) The mesh around a reconstructed grain, colored by the absolute value of the mean grain boundary curvature. (D) The same grain in (C) but colored by the grain boundary normal direction [Color figure can be viewed at wileyonlinelibrary.com]

the boundaries, are illustrated in Figure 1. There are a total of 3032 grains. If we define bulk grains as those whose centroids are separated from the nearest free surface by more than the average grain diameter, then there are 887 bulk grains. The average (spherical equivalent) grain diameter, D, is 3.33 μm, but it is clear from the images that the grain size distribution is not normal. The largest grain in the sample has a diameter of 14.5 μm, which is more than four times the average. The average number of neighbors per grain (taken to be equivalent to the number of grain faces, F), is 11.9. The distributions of grain sizes and grain faces are shown in Figure 2A,B, respectively. In both cases, the main part of the distribution appears normal, but the tails extend to higher than expected values. To show the distributions more clearly, a few very large grains with many sides were excluded. When these distributions are compared, as in Figure 2C, it is apparent that the grain size and the number of grain faces are correlated such that the larger (smaller) grains tend to have more (fewer) faces. This is consistent with observations reported for other materials.[13,31]

The integral mean curvature of grain faces was calculated for each bulk grain by summing the products of the area and curvature for every triangle bounding a given grain. The integral mean curvature of grain faces will be referred as the integral curvature in the remaining text for readability purpose. However, we note here that the curvature at triple lines and quadruple points were not considered in any calculations of this paper. In Figure 3, the values of M_s for every grain have been classified by grain size. Each point is the average of M_s in that size class and the bar shows the standard deviation of M_s within that size class (note that, for clarity, six grains with diameters

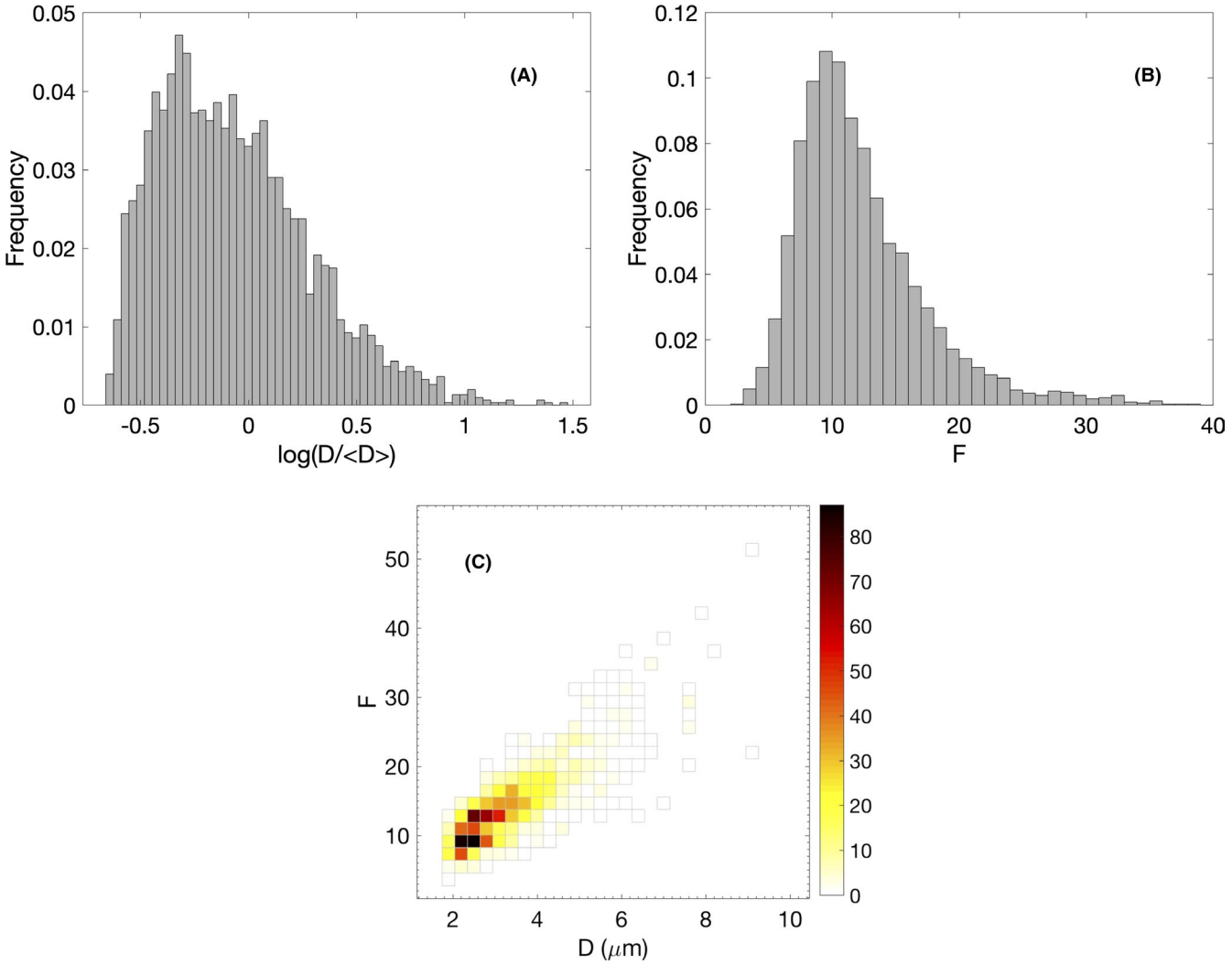

FIGURE 2 The distributions of diameters and numbers of faces in $SrTiO_3$. (A) Grain size distribution. (B) Distribution of the number of grain faces. (C) The relationship between the grain diameter and the number of grain faces. In each category, the color indicates number of grains in this category [Color figure can be viewed at wileyonlinelibrary.com]

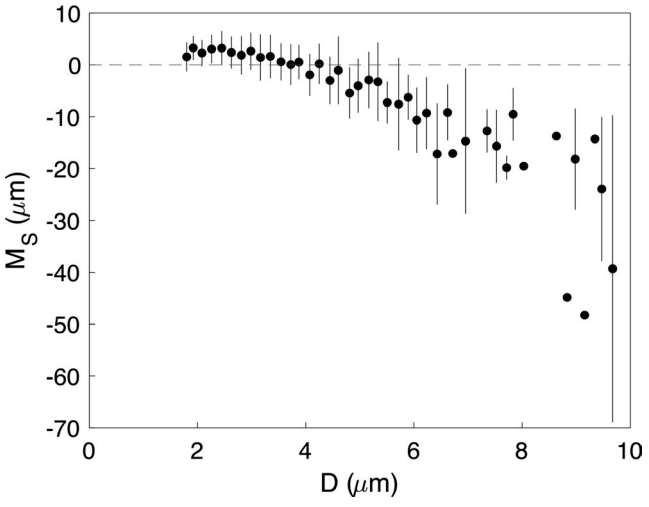

FIGURE 3 Integral mean curvature (M_s) of grains as a function of the spherical equivalent grain diameter. For each category, the circle is the mean value and the line shows one standard deviation

larger than 10 μm were excluded from this plot). A clear trend appears that smaller grains have positive curvatures (are convex) and larger grains have negative curvatures (are concave). The cross over from positive to negative curvature occurs for grains with diameters of about 3.8 μm, which is greater than the mean diameter (3.3 μm). With reference to Figure 2A, this shows that the majority of grains have positive curvature. Because grain boundaries move toward their centers of curvature, the smaller convex grains should tend to shrink and the larger concave grains should tend to grow. However, note that within each size class, there is a range of curvatures and in many cases the distribution spans positive and negative curvatures. This might arise from uncertainties in the measurement, but it also might arise from local fluctuations in curvature that depend on a grain's neighbors.[38] If so, then not all grains of the same equivalent diameter have the same sign of curvature. The largest grains have

strongly negative curvatures and are expected to grow and consume the smaller grains.

Considering the relationship between the grain size and the number of grain faces illustrated in Figure 2C, a similar relation between curvature and number of grain faces should be observed. Figure 4A shows the average and standard deviation of integral mean curvatures for grains with different numbers of faces (note that, for clarity, nine grains with more than 40 faces were excluded from this plot). The mean values of M_s are positive for grains with fewer than 16 sides and the mean values of M_s are negative for grains with 16 or more sides. However, as before, there are a range of classes (between 11 and 21 faces) where both positive and negative values fall within one standard deviation of the mean. The results in Figure 4A affirm the well known connection between the number of grain faces and the curvature, that grains with few (many) faces have positive (negative) curvatures, are convex (concave), and are likely to shrink (grow).[39–41] The distribution of integral mean curvatures in each topology class suggests that the number of grain faces alone does not uniquely determine the integral curvature for 3D grains. This is in contrast to a 2D isotropic model, where the number of neighbors determines the curvature.

It has been previously suggested that the grains with zero curvature are those whose numbers of faces (F) are the same as the average numbers of faces of their nearest neighbors, $<F_{NN}>$.[13] We therefore define the number of excess faces as $F - <F_{NN}>$. Using data for β-Ti,[13] an austenitic steel,[16] and phase field grown microstructures[42] this proposition was shown to be true, at least on average. Figure 4B presents the current curvature measurements as a function of $F - <F_{NN}>$. Here, we use the normalized integral mean curvature ($\mathcal{G}'$), which is determined from the integral mean curvature and the spherical equivalent grain radius (R): $\mathcal{G}' = M_s/R$. As pointed out in Ref. [13], only grains whose nearest neighbors are all unbiased, namely centroids separated from the nearest free surface by more than the average grain diameter, can be considered in the analysis of $<F_{NN}>$. However, when this condition was enforced, too few grains remained for the analysis. We conducted the $F - <F_{NN}>$ analysis with the 887 grains used in Figures 3 and 4A, which are unbiased themselves but may have biased neighbors. It is interesting to note that the correlation between $\mathcal{G}'$ and $F - <F_{NN}>$ is actually robust even though biased neighboring grains were included. In Figure 4B, the individual grain data points are shown as gray circles and the averaged values for each topology class ($F - <F_{NN}>$) are shown as red squares. It can be seen that for the class averaged values, $\mathcal{G}'$ and $F - <F_{NN}>$ are almost linearly correlated and a fitted line will pass through the origin almost exactly. We conclude that the close correlation between and $F - <F_{NN}>$ previously observed in metals[13,16] also occurs in this ceramic.

The distributions of the relative areas of grain boundaries, their relative energies, and their curvatures, when classified by crystallography, show correlations. In Figure 5, the relative energies, areas, and absolute mean curvatures are plotted as function of the orientation of the grain boundary plane, ignoring the boundary misorientation. The distribution of grain boundary planes, illustrated in Figure 5B, shows a preference for grain boundaries with (100) orientations and the minimum at (111). This is consistent with earlier measurements.[17,19] The relative grain boundary energy (Figure 5C) is lowest at (100) and highest at (111). This inverse relationship between the relative grain

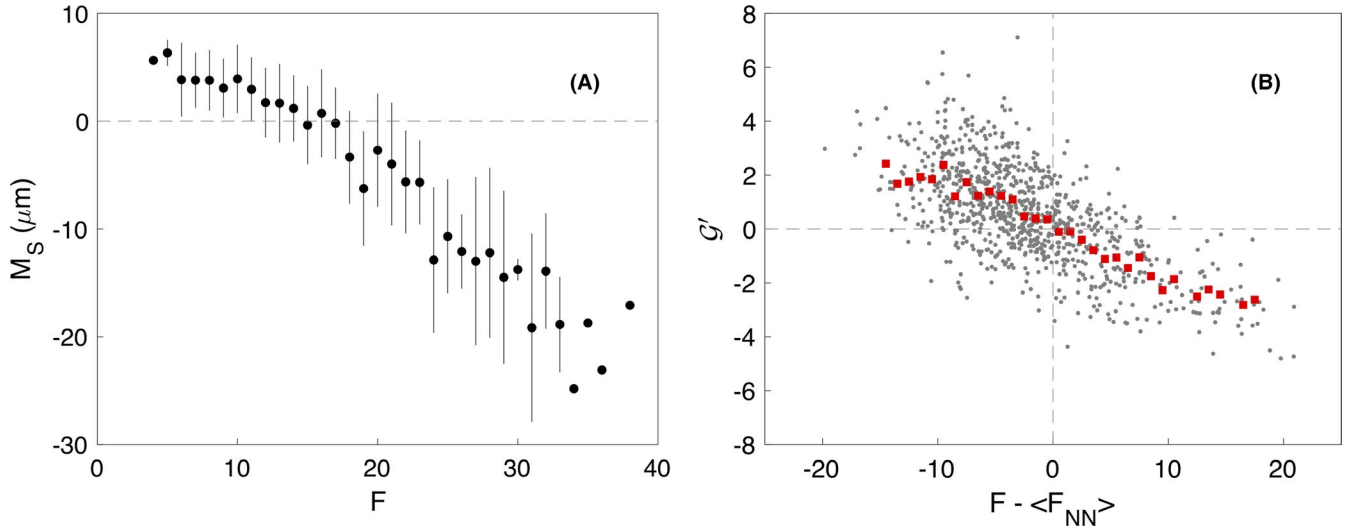

FIGURE 4 (A) Integral mean curvature (M_s) of grain faces as a function of the number of grain faces, F, for each grain. For each category, the circle is the mean values and the line shows one standard deviation. (B) Normalized integral curvature of grain faces ($\mathcal{G}'$) as a function of $F - <F_{NN}>$. $F - <F_{NN}>$ is the difference between the number of faces of one grain (F) and the average number of faces of its nearest neighbors ($<F_{NN}>$) [Color figure can be viewed at wileyonlinelibrary.com]

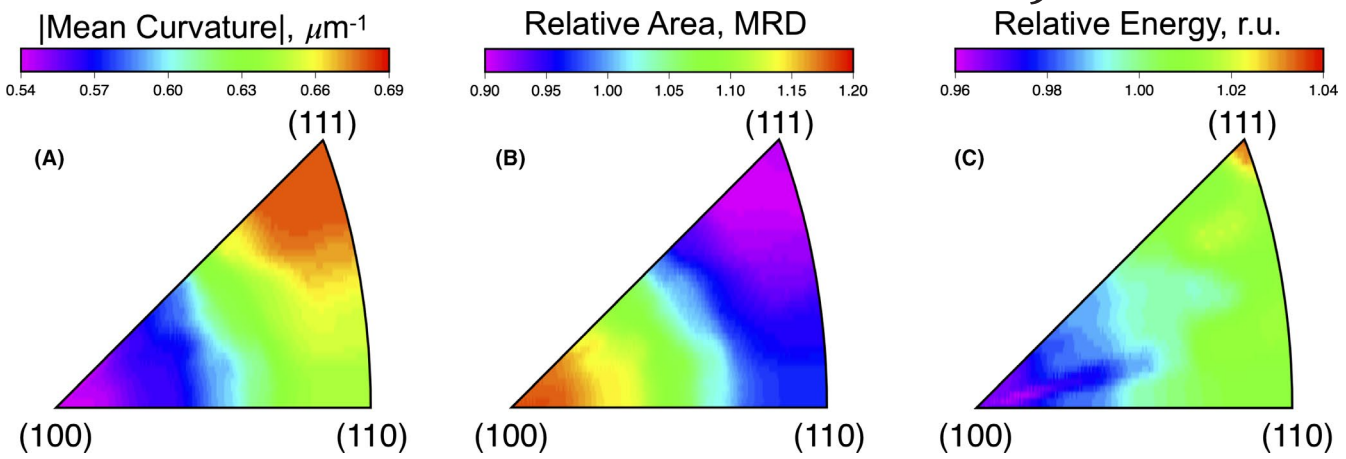

FIGURE 5 Variations of grain boundary properties, plotted as a function of grain boundary plane orientation (ignoring the grain boundary misorientation) [Color figure can be viewed at wileyonlinelibrary.com]

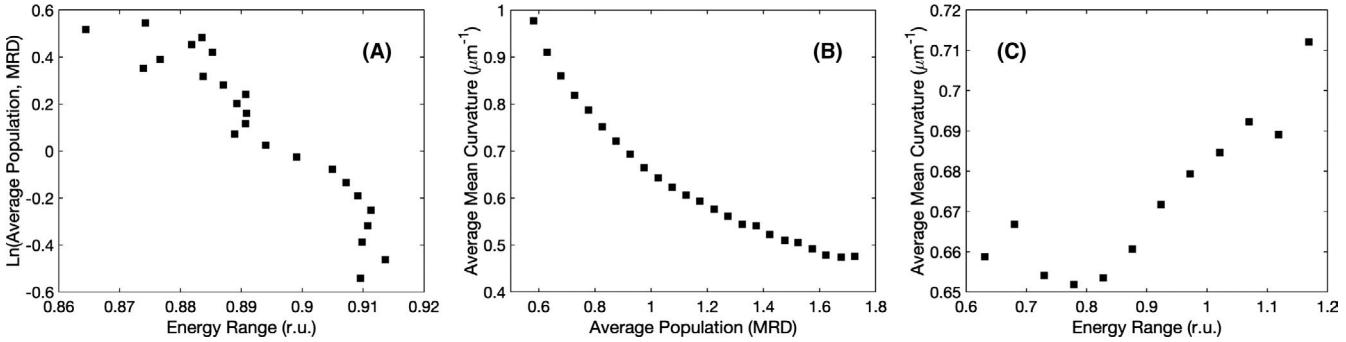

FIGURE 6 Correlations between average values of grain boundary properties. (A) The average energies of all boundaries in a 0.05 MRD range of relative area. (B) The average curvatures of all boundaries in a 0.05 MRD range of relative area. (C) The average curvatures of all boundaries in a 0.05 r.u. range of relative energy. In each plot, only averages determined from at least three observations are included. The standard deviations of the average energies in (A) and curvatures in (B) and (C) are 0.2 r.u., 0.12 and 0.08 μm^{-1}, respectively

boundary area and energy is consistent with measurements of other polycrystals that evolved by grain growth.[3,37,43] The absolute value of the curvature also depends on the orientation of the grain boundary plane. In this case, the minimum curvature is at the (100) orientation and the maximum curvature is at the (111) orientation. These results show a direct correlation between the curvature and the energy and an inverse correlation between the curvature and the relative grain boundary area. As an example, faces of a single grain with these characteristics are shown in Figure 1C,D. The black arrows indicate two grain faces with mostly (100) orientations and low curvature. Such flat (100) faces are common in the microstructure and have been observed in several experimental studies.[26,44] The yellow arrow indicates a grain face with (110) orientations and relatively high curvature.

The correlations suggested by the results in Figure 5 can be tested. Specifically, we can determine the average value of one property for all of the boundaries that have a second property within a certain range. For example, when we average the energies of all grain boundaries that have relative areas within a 0.05 MRD range, the correlation in Figure 6A is obtained. Note that although there is some scatter, there is an inverse correlation between the quantities. When the curvatures of all boundaries within a 0.05 MRD range are averaged, there is also an inverse correlation (see Figure 6B). When the curvatures of all boundaries within a 0.05 r.u. range of the relative energy are averaged (Figure 6C), there is a positive correlation over the majority of the domain (>0.8 r.u.). All three of these trends are consistent with the trends observed in Figure 5.

It is also possible to examine these grain boundary properties as a function of grain boundary plane orientation at a fixed misorientation and one example is illustrated in Figure 7. The relative areas of different grain boundary planes are shown in Figure 7B. The maxima in the distribution are centered on the orientations of the symmetric tilt boundaries at (031) and $(0\bar{1}3)$. The secondary maxima are at the (100) and $(\bar{1}00)$ orientations. Being perpendicular to the misorientation axis, they are twist boundaries. An energy minimum (see Figure 7C) is

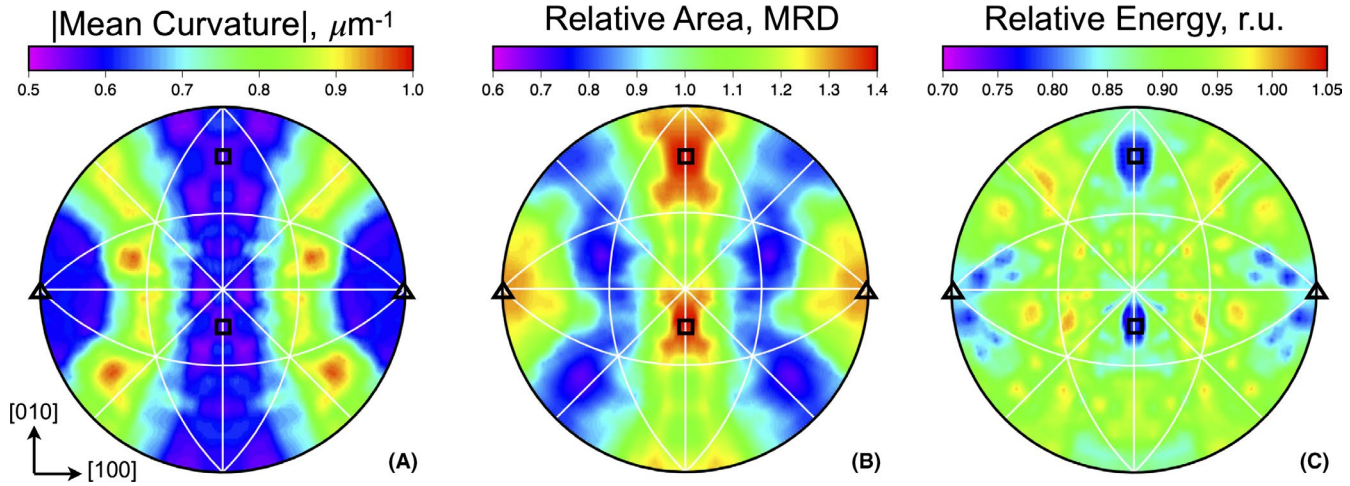

FIGURE 7 The (A) curvatures, (B) relative areas, and (C) relative energies as a function of grain boundary plane orientation for boundaries with a 40° misorientation around [100]. Each distribution is plotted in stereographic projection. The (031) and (0$\bar{1}$3) orientations are marked by black squares and the (100) and ($\bar{1}$00) positions are marked with triangles. This is also the position of the misorientation axis [Color figure can be viewed at wileyonlinelibrary.com]

also at the symmetric tilt grain boundary position and there are other local energy minima near the twist grain boundary positions, consistent with the inverse correlations evident in Figures 5 and 6. The low curvatures at the twist boundary positions and the symmetric tilt positions are consistent with the correlation to energy and inverse correlation to area in Figures 5 and 6. The examination of the distributions at other misorientations (not shown) exhibit similar trends.

4 | DISCUSSION

The results for the integral mean curvature as a function of the grain size (Figure 3) and the number of faces (Figure 4A) vary in such a way that on average small grains, with 16 or fewer faces, have positive curvature and are therefore convex. Larger grains with more than 16 faces on average have negative curvatures and are therefore concave. It should be noted that the sign of the integral mean curvature does not imply that the curvature of every face has the same sign; it represents the net curvature. These results are similar to results previously published for β-Ti[13] and two ferrous alloys,[16] suggesting that there are no significant differences in the relation between the neighborhood topology and curvature for metallic and ceramic polycrystals. If one compares the distribution of grains as a function of the number of sides (Figure 2B) and the integral mean curvature as a function of the number of sides (Figure 4A), it is clear that far more grains have positive curvature than have negative curvature. Therefore, more grains are convex and, presumably, shrinking than there are concave (negative curvature) growing grains. By conservation, all volume lost from shrinking grains must be gained by growing grains. Interestingly, when we plot the cumulative volume as a function of the number of sides (see Figure 8) using all 3032 grains within the two sample volumes, we see that 50% of the total volume is in grains with more than 16 neighbors. So, while there are fewer concave grains with more than 16 neighbors, they are on average larger than the grains with fewer than 16 neighbors.

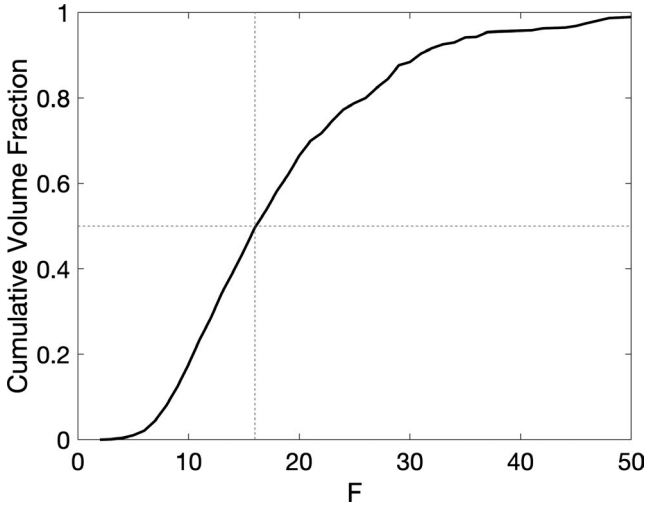

FIGURE 8 Cumulative fraction of the total volume of grains when classified according to number of neighbors. The dashed lines mark the position of ½ of the cumulative volume fraction and 16 neighbors

Given the relationships between grain size, number of neighbors, and integral mean curvature, one might assume that the correlation between curvature and grain boundary crystallography would be weak. However, Figures 5A and 7A show that this is not the case. It is important to emphasize that the curvatures in these figures were classified only by

crystallography, meaning that the value at every orientation is the average of data from grains of all sizes. In other words, grain boundaries with (100) orientations have lower curvatures (are flatter) on average then boundaries of (111) orientation, regardless of the size of the grain. Note that this is an unsigned curvature. Because of grain exchange symmetry, the sign of the boundary curvature is not unique. If a grain boundary is convex in the reference frame of one grain, it is concave in the indistinguishable reference frame of the other. The fact that the crystallographic correlation is independent of grain sizes arises because of the requirement that single boundaries join large and small grains.

A possible explanation for the relationship between a grain boundary's curvature and crystallography is the tendency of an interface to have a uniform chemical potential when local equilibrium occurs in the microstructure. Herring[1] defined the chemical potential of a nonsingular interface (μ_{ns}) as:

$$\mu_{ns} = \left(\gamma + \frac{\partial^2 \gamma}{\partial \theta_1^2}\right)\kappa_1 + \left(\gamma + \frac{\partial^2 \gamma}{\partial \theta_2^2}\right)\kappa_2 \quad (4)$$

If we ignore the second derivatives and define the mean curvature as $H = 1/2(\kappa_1 + \kappa_2)$, then Equation 4 reduces to the simplified form:

$$\mu_{ns} = 2H\gamma \quad (5)$$

Assuming that there is a mean field chemical potential, and individual interfaces have chemical potentials that approximate this value, then Equation 5 indicates that the curvature and the energy should be inversely related. This is reasonable, because curvature increases the interface area and the energy penalty for this curvature increases with the energy of the boundary. However, this is not consistent with the data, which shows curvature and energy to be directly proportional.

The observations that H and γ are not inversely related suggest that these boundaries may not be continuously curved surfaces. Evidence for the existence of facets can be found in Figure 7C, where there are abrupt minima in the grain boundary at the positions of the symmetric tilt and twist boundaries. If a grain boundary were made of singular interfaces, then there is a different prescription for determining the chemical potential, which was described by Herring[1] and Taylor.[45] For the case of singular interfaces, κ is undefined and γ is not differentiable, so Equation 4 is inoperable. When a singular (flat) interface moves along its normal, the change in energy occurs at the periphery of the facet and to the boundaries connected at the periphery, as illustrated schematically in Figure 9. We illustrate this point in the next paragraph.

Imagine a ridge that is infinitely long in the y direction, as in Figure 9. We can describe its energy change per unit length in the y direction when the flat top surface moves in the z direction. As illustrated in Figure 9, this hypothetical ridge is bounded by three facets of two types. The top facet is of type 2. The left and right facets are of type 1. If the top facet in Figure 9A moves downward by Δz, its area increases by $A' - = 2\delta\sigma_2$. At the same time, some area of the lateral type 1 facets ($2\delta\sigma_1$) is eliminated. The exact energy change $\left(2\delta\sigma_2\gamma_2\Delta z\cot(\theta) - 2\delta\sigma_1\gamma_1\Delta z/\sin(\theta)\right)$depends on the energies of σ_1 and σ_2 (γ_1 and γ_2), the distance the facet moves (Δz), and the angle between the facets (θ). This illustrates the key difference between the energy changes that occur during the motion of a singular and nonsingular boundary. For the nonsingular case, the energy change is determined completely by the radius of curvature and the energy of the grain boundary of interest. For the singular case, it is determined by the details of the specific geometry (θ in the simplified case illustrated in Figure 9) through the weighted mean curvature[45] and the boundary energy of both the boundary of interest and peripheral boundaries. In polycrystalline microstructures, a grain boundary, singular or nonsingular, is usually connected to many different types of grain boundaries,

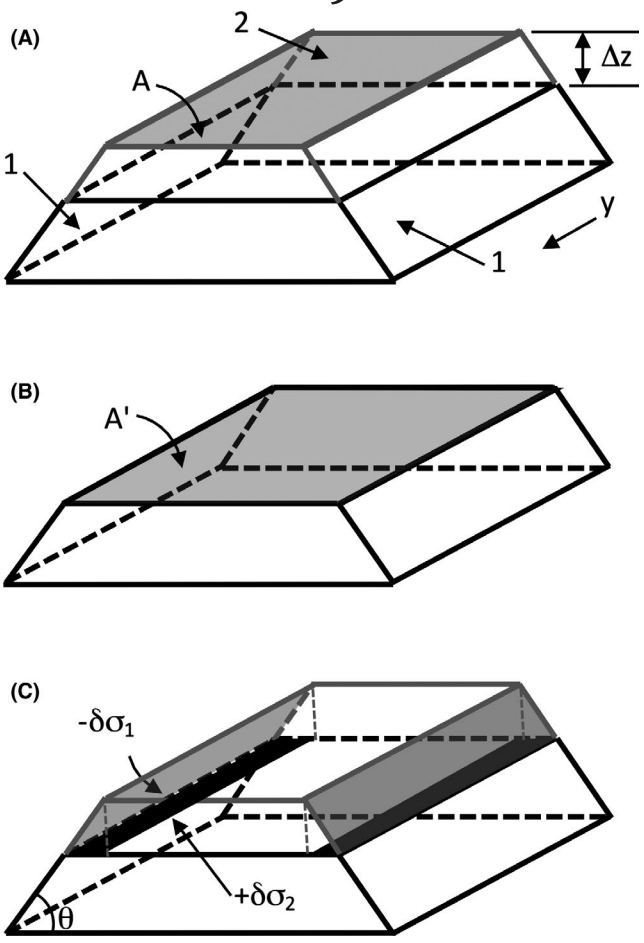

FIGURE 9 Schematic of a ridge, assumed to extend infinitely in the + and −y directions, formed when two surfaces of type 1 meet a surface of type 2. (A) Initial position. (B) After surface 2 retracts by an amount Δz. (C) Illustration of the changes in the surface area

although the types of these neighbors are not completely random.[46] Considering all of the possibilities for θ, γ_1, and γ_2, it is difficult to draw a general conclusion about the relation between measured curvature and energy in the presence of singular interfaces. If such boundaries are present in larger numbers, it is not surprising that the inverse correlation between curvature and energy is not observed.

If the $SrTiO_3$ grain boundary network were dominated by singular interfaces, we have a reasonable idea about what we would observe in our experiment. First, we will not measure zero curvature. The discretized nature of the data and the meshing of the boundary will lead to a minimum but finite curvature. Second, we would also measure energy minima at these orientations. In other words, low energy would correlate with low curvature, as we observe. Another consideration is that if the interfaces were mostly singular, one might expect a finite number of interfaces, but instead we observe a continuous range of interface orientations. This difference can be reconciled if the boundaries are faceted on a length scale smaller than the resolution of the EBSD maps. In this case, we would see a continuous range of orientations even if the boundaries were composed of different combinations of more elementary orientations. In fact, there is TEM evidence that is consistent with that idea. Sternlicht et al[27,28] reported that, regardless of the macroscopic boundary orientation, on the microscopic level grain boundaries in $SrTiO_3$ are made up of nanometer-scale flat terraces that mostly have {100} and {110} orientations separated by steps that also create {100} and {110} orientations. The steps in the micrographs are larger than the minimal possible step heights, usually by a small integer multiple, but it is not obvious that they could be considered facets. However, migration of such boundaries would require changing the areas of both the larger atomically flat terraces and the smaller multi-layer steps by a process analogous to that illustrated in Figure 9.

The observation that grain boundaries are microscopically made up of more elementary low-index orientations is not inconsistent with surface observations. Relative surface energies are found to be reasonable predictors of relative grain boundary energies[19,47,48] and it has been reported that in this temperature range, $SrTiO_3$ surfaces are fully faceted and made up of low-index orientations.[17]

Finally, it is worth noting that these measurements are consistent with changes that are observed for $SrTiO_3$ grain boundaries in the so-called "anti-thermal" region where the boundaries migrate more slowly.[22] Measurements have shown that there is an increase in boundaries with low energy and with the (100) orientation.[17,25] Here, we find these (100)-oriented, low energy boundaries also have a minimum curvature. Therefore, they have the lowest driving force for migration. While this does not explain why such low curvature, low energy boundaries form in this temperature range, it is consistent with the phenomenological observation of slower grain boundary migration.

5 | CONCLUSIONS

Using 3D EBSD, we have measured the distribution of relative areas, energies, and curvatures in $SrTiO_3$ annealed at 1470°C. The integral mean curvatures of grains vary such that small grains with fewer than 16 sides have positive curvatures and larger grains with more than 16 sides have negative curvatures. The number of excess neighbors correlates strongly with the normalized integral mean curvature. The curvature is positive (negative) if a grain has fewer (more) neighbors than the average of its neighbors. The grain boundary curvature is inversely correlated to the grain boundary area, such that flat boundaries make up a relatively larger portion of the grain boundary area. Also, grain boundary curvature is correlated to grain boundary energy, such that lower energy boundaries are flatter and relatively larger. This latter correlation suggests that the grain boundary network is dominated by singular boundaries.

ACKNOWLEDGMENTS

G.S.R. acknowledges support from the National Science Foundation under grant DMR 1628994 and, for equipment, MRI grant DMR 1428480. X.Z. acknowledges support from the W.M. Keck Foundation. The authors acknowledge use of the Materials Characterization Facility at Carnegie Mellon University supported by grant MCF-677785.

ORCID

Xiaoting Zhong https://orcid.org/0000-0002-1636-4939
Shen J. Dillon https://orcid.org/0000-0002-6192-4026
Gregory S. Rohrer https://orcid.org/0000-0002-9671-3034

REFERENCES

1. Herring C. The use of classical macroscopic concepts in surface energy problems. In: Gomer R, Smith CS, editors. Structure and properties of solid surfaces; proceedings of a conference arranged by the National Research Council and held. September, 1952, in Lake Geneva, Wisconsin, USA. Chicago: University of Chicago Press, 1953; pp. 5–81.
2. Mullins WW. Capillarity-induced surface morphologies. Int Sci. 2001;9(1–2):9–20.
3. Rohrer GS. Grain boundary energy anisotropy: a review. J Mater Sci. 2011;46(18):5881–95.
4. Molodov DA, Czubayko U, Gottstein G, Shvindlerman LS. Mobility of 111 tilt grain-boundaries in the vicinity of the special misorientation sigma=7 in bicrystals of pure aluminum. Scripta Metall Mater. 1995;32(4):529–34.
5. Upmanyu M, Srolovitz DJ, Shvindlerman LS, Gottstein G. Misorientation dependence of intrinsic grain boundary mobility: simulation and experiment. Acta Mater. 1999;47(14):3901–14.
6. Winning M, Rollett AD, Gottstein G, Srolovitz DJ, Lim A, Shvindlerman LS. Mobility of low-angle grain boundaries in pure metals. Phil Mag. 2010;90(22):3107–28.

7. Abdeljawad F, Foiles SM, Moore AP, Hinkle AR, Barr CM, Heckman NM, et al. The role of the interface stiffness tensor on grain boundary dynamics. Acta Mater. 2018;158:440–53.
8. Demirel MC, Kuprat AP, George DC, Rollett AD. Bridging simulations and experiments in microstructure evolution. Phys Rev Lett. 2003;90(1):016106.
9. McKenna IM, Poulsen SO, Lauridsen EM, Ludwig W, Voorhees PW. Grain growth in four dimensions: a comparison between simulation and experiment. Acta Mater. 2014;78:125–34.
10. Alkemper J, Voorhees PW. Three-dimensional characterization of dendritic microstructures. Acta Mater. 2001;49(5):897–902.
11. Mason JK. Grain boundary energy and curvature in Monte Carlo and cellular automata simulations of grain boundary motion. Acta Mater. 2015;94:162–71.
12. Patterson BR, Rowenhorst DJ, Tikare V, DeHoff RT, Kaub TM. Affinities for topological arrangements in grain structures. Acta Mater. 2014;79:411–20.
13. Rowenhorst DJ, Lewis AC, Spanos G. Three-dimensional analysis of grain topology and interface curvature in a beta-titanium alloy. Acta Mater. 2010;58(16):5511–9.
14. Rowenhorst DJ, Voorhees PW. Measurement of Interfacial Evolution in Three Dimensions. Ann Rev Mater Res. 2012;42:105–24.
15. Zhang J, Zhang YB, Ludwig W, Rowenhorst D, Voorhees PW, Poulsen HF. Three-dimensional grain growth in pure iron. Part I. statistics on the grain level. Acta Mater. 2018;156:76–85.
16. Zhong X, Rowenhorst DJ, Beladi H, Rohrer GS. The five-parameter grain boundary curvature distribution in an austenitic and ferritic steel. Acta Mater. 2017;123:136–45.
17. Rheinheimer W, Baeurer M, Chien H, Rohrer GS, Handwerker CA, Blendell JE, et al. The equilibrium crystal shape of strontium titanate and its relationship to the grain boundary plane distribution. Acta Mater. 2015;82:32–40.
18. Sano T, Saylor DM, Rohrer GS. Surface energy anisotropy of $SrTiO_3$ at 1400 degrees C in air. J Am Ceram Soc. 2003;86:1933–9.
19. Saylor DM, El Dasher B, Sano T, Rohrer GS. Distribution of grain boundaries in $SrTiO_3$ as a function of five macroscopic parameters. J Am Ceram Soc. 2004;87(4):670–6.
20. Rheinheimer W, Baeurer M, Handwerker CA, Blendell JE, Hoffmann MJ. Growth of single crystalline seeds into polycrystalline strontium titanate: anisotropy of the mobility, intrinsic drag effects and kinetic shape of grain boundaries. Acta Mater. 2015;95:111–23.
21. Rheinheimer W, Baeurer M, Hoffmann MJ. A reversible wetting transition in strontium titanate and its influence on grain growth and the grain boundary mobility. Acta Mater. 2015;101:80–9.
22. Rheinheimer W, Hoffmann MJ. Non-Arrhenius behavior of grain growth in strontium titanate: new evidence for a structural transition of grain boundaries. Scripta Mater. 2015;101:68–71.
23. Rheinheimer W, Hoffmann MJ. Grain growth in perovskites: what is the impact of boundary transitions? Curr Opin Solid State Mater Sci. 2016;20(5):286–98.
24. Rheinheimer W, Hoffmann MJ. Grain growth transitions of perovskite ceramics and their relationship to abnormal grain growth and bimodal microstructures. J Mater Sci. 2016;51(4):1756–65.
25. Kelly MN, Rheinheimer W, Hoffmann MJ, Rohrer GS. Anti-thermal grain growth in $SrTiO_3$: coupled reduction of the grain boundary energy and grain growth rate constant. Acta Mater. 2018;149:11–8.
26. Shih S-J, Lozano-Perez S, Cockayne DJH. Investigation of grain boundaries for abnormal grain growth in polycrystalline $SrTiO_3$. J Mater Res. 2010;25(2):260–5.
27. Sternlicht H, Rheinheimer W, Dunin-Borkowski RE, Hoffmann MJ, Kaplan WD. Characterization of grain boundary disconnections in $SrTiO_3$ part I: the dislocation component of grain boundary disconnections. J Mater Sci. 2019;54(5):3694–709.
28. Sternlicht H, Rheinheimer W, Hoffmann MJ, Kaplan WD. The mechanism of grain boundary motion in $SrTiO_3$. J Mater Sci. 2016;51(1):467–75.
29. Dillon SJ, Rohrer GS. Characterization of the grain-boundary character and energy distributions of yttria using automated serial sectioning and EBSD in the FIB. J Am Ceram Soc. 2009;92(7):1580–5.
30. Groeber MA, Jackson MADREAM. 3D: a digital representation environment for the analysis of microstructure in 3D. Integrating materials and manufacturing. Innovation. 2014;3:5.
31. Kelly MN, Glowinski K, Nuhfer NT, Rohrer GS. The five parameter grain boundary character distribution of alpha-Ti determined from three-dimensional orientation data. Acta Mater. 2016;111:22–30.
32. Goldfeather J, Interrante V. A novel cubic-order algorithm for approximating principal direction vectors. ACM Trans Graph. 2004;23(1):45–63.
33. Morawiec A. Method to calculate the grain boundary energy distribution over the space of macroscopic boundary parameters from the geometry of triple junctions. Acta Mater. 2000;48(13):3525–32.
34. Herring C. Surface tension as a motivation for sintering. In: The physics of powder metallurgy. Kingston WE (ed). New York: McGraw-Hill; 1951: p. 36.
35. Cahn JW, Hoffman DW. Vector thermodynamics for anisotropic surfaces 2. Curved and faceted surfaces. Acta Metall. 1974;22(10):1205–14.
36. Hoffman DW, Cahn JW. Vector thermodynamics for anisotropic surfaces 1. Fundamentals and application to plane surface junctions. Surf Sci. 1972;31(1):368–88.
37. Saylor DM, Morawiec A, Rohrer GS. Distribution and energies of grain boundaries in magnesia as a function of five degrees of freedom. J Am Ceram Soc. 2002;85(12):3081–3.
38. Bhattacharya A, Shen YF, Hefferan CM, Li SF, Lind J, Suter RM, et al. Three-dimensional observations of grain volume changes during annealing of polycrystalline Ni. Acta Mater. 2019;167:40–50.
39. MacPherson RD, Srolovitz DJ. The von Neumann relation generalized to coarsening of three-dimensional microstructures. Nature. 2007;446(7139):1053–5.
40. Mullins WW. 2-Dimensional motion of idealized grain boundaries. J Appl Phys. 1956;27(8):900–4.
41. Mullins WW. Estimation of the geometrical rate-constant in idealized 3 dimensional grain-growth. Acta Metall. 1989;37(11):2979–84.
42. Yadav V, Moelans N. Analysis of grain topology and volumetric growth rate relation in three-dimensional normal grain growth. Acta Mater. 2018;156:275–86.
43. Beladi H, Rohrer GS. The relative grain boundary area and energy distributions in a ferritic steel determined from three-dimensional electron backscatter diffraction maps. Acta Mater. 2013;61(4):1404–12.

44. Syha M, Rheinheimer W, Baurer M, Lauridsen EM, Ludwig W, Weygand D, et al. Three-dimensional grain structure of sintered bulk strontium titanate from X-ray diffraction contrast tomography. Scripta Mater. 2012;66(1):1–4.
45. Taylor JE. Mean-curvature and weighted mean-curvature. 2. Acta Metall Mater. 1992;40(7):1475–85.
46. Miyazawa K, Iwasaki Y, Ito K, Ishida Y. Combination rule of Sigma values at triple junctions in cubic polycrystals. Acta Cryst A. 1996;52:787–96.
47. Sutton AP. An ananlytic model for grain-boundary expansions and cleavage energies. Phil Mag A. 1991;63(4):793–818.
48. Wolf D. Correlation between structure, energy, and ideal cleavage fracture for symmetrical grain-boundaries in fcc metals. J Mater Rese. 1990;5(8):1708–30.

SUPPORTING INFORMATION

Additional supporting information may be found online in the Supporting Information section at the end of the article.

How to cite this article: Zhong X, Kelly MN, Miller HM, Dillon SJ, Rohrer GS. Grain boundary curvatures in polycrystalline $SrTiO_3$: Dependence on grain size, topology, and crystallography. *J Am Ceram Soc*. 2019;102:7003–7014. https://doi.org/10.1111/jace.16608